AJNR

Dual-Energy Parathyroid 4D-CT: Improved Discrimination of Parathyroid Lesions from Thyroid Tissue Using Noncontrast 40-keV Virtual Monoenergetic Images

P.M. Bunch, A.A. Pavlina, M.E. Lipford and J.R. Sachs

AJNR Am J Neuroradiol 2021, 42 (11) 2001-2008
doi: https://doi.org/10.3174/ajnr.A7265
http://www.ajnr.org/content/42/11/2001

Dual-Energy Parathyroid 4D-CT: Improved Discrimination of Parathyroid Lesions from Thyroid Tissue Using Noncontrast 40-keV Virtual Monoenergetic Images

P.M. Bunch, A.A. Pavlina, M.E. Lipford, and J.R. Sachs

ABSTRACT

BACKGROUND AND PURPOSE: In parathyroid CT, a noncontrast phase aids discrimination of parathyroid lesions (not iodine-containing) from thyroid tissue (iodine-containing). When thyroid iodine is pathologically diminished, this differentiation is difficult with standard CT. Because the attenuation of an element is maximal near its K-edge (iodine = 33.2 keV), we hypothesized that dual-energy CT 40-keV virtual monoenergetic images will accentuate thyroid iodine relative to standard images, improving the differentiation of thyroid from parathyroid lesions. Our purpose was to test this hypothesis through quantitative assessment of Hounsfield unit attenuation and contrast-to-noise on dual-energy CT standard (70-keV) and 40-keV noncontrast images.

MATERIALS AND METHODS: For this retrospective study including 20 dual-energy parathyroid CTs, we used an ROI-based analysis to assess the attenuation of thyroid tissue, parathyroid lesions, and sternocleidomastoid muscle as well as corresponding contrast-to-noise on standard and 40- keV noncontrast images. Wilcoxon signed rank tests were performed to compare differences between 70 and 40 keV.

RESULTS: Absolute and percentage increases in attenuation at 40 keV were significantly greater for thyroid gland than for parathyroid lesions and sternocleidomastoid muscle ($P < .001$ for all). Significant increases in the contrast-to-noise of thyroid relative to parathyroid lesions (median increase, 0.8; $P < .001$) and relative to sternocleidomastoid muscle (median increase, 1.3; $P < .001$) were observed at 40 keV relative to 70 keV.

CONCLUSIONS: Forty-kiloelectron volt virtual monoenergetic images facilitate discrimination of parathyroid lesions from thyroid tissue by significantly increasing thyroid attenuation and associated contrast-to-noise. These findings are particularly relevant for parathyroid lesions that exhibit isoattenuation to the thyroid on parathyroid CT arterial and venous phases and could, therefore, be missed without the noncontrast phase.

ABBREVIATIONS: CNR = contrast-to-noise ratio; DECT = dual-energy CT; IQR = interquartile range; VMI = virtual monoenergetic images

Parathyroid 4D-CT is a powerful tool for localizing abnormal parathyroid tissue in the setting of primary hyperparathyroidism.[1] Localization of a single adenoma facilitates minimally invasive parathyroidectomy and its associated benefits,[2,3] whereas localization of multigland disease aids bilateral neck exploration. The optimal number of CT phases is undetermined, but the most commonly used protocol involves 3 CT acquisitions of the neck and upper chest, including noncontrast, arterial, and venous phases.[4]

Parathyroid lesions, exophytic thyroid nodules, and lymph nodes may appear morphologically identical on CT.[5] Although the classic postcontrast enhancement pattern of parathyroid adenomas is well-described (hyperattenuating relative to thyroid on arterial phase images; hypoattenuating [washout] relative to thyroid on venous phase images), a challenge for the radiologist is that this classic pattern is seen in only 20% of adenomas.[6] Moreover, it is estimated that up to 25% of parathyroid lesions could be missed without the noncontrast CT phase.[6] Parathyroid lesions are always lower in attenuation than the normal, iodine-containing thyroid gland on noncontrast images.[1] However, another challenge for the radiologist is that thyroid disease and primary hyperparathyroidism frequently coexist,[7,8] and chronic thyroid disease (eg, Hashimoto disease) can result in abnormal hypoattenuation of the thyroid gland related to diminished iodine content (Fig 1).[1] In such cases, using the noncontrast images to differentiate parathyroid lesions from the abnormally hypoattenuating thyroid gland is more difficult.

Numerous applications of dual-energy CT (DECT) have been described for neuroradiology practice.[9] Low-keV (eg, 40 keV)

Received January 15, 2021; accepted after revision June 8.

From the Department of Radiology, Wake Forest School of Medicine, Winston Salem, North Carolina.

A scientific abstract related to the work represented in this article was presented at: Annual Meeting of the American Society of Neuroradiology, May 22–26. 2021; Virtual.

Please address correspondence to Paul M. Bunch, MD, Department of Radiology, Wake Forest School of Medicine, Medical Center Boulevard, Winston Salem, NC 27157; e-mail: paul.m.bunch@gmail.com; @pbunchmd

http://dx.doi.org/10.3174/ajnr.A7265

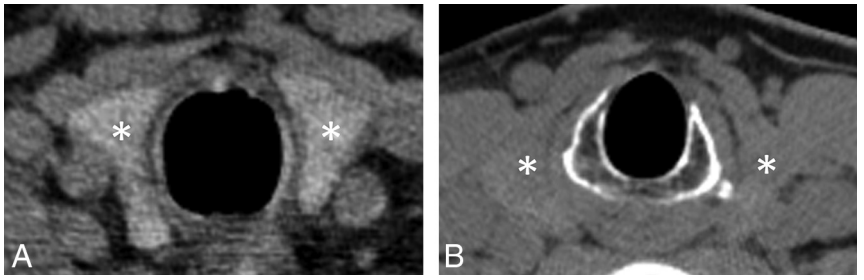

FIG 1. Axial, noncontrast, single-energy CT image (*A*) obtained in a patient with normal thyroid function demonstrates the normal hyperattenuating appearance of the thyroid gland (*asterisks*, *A*) relative to adjacent soft tissue. When present, this normal hyperattenuating appearance enables differentiation of parathyroid lesions adjacent to the thyroid gland from exophytic thyroid tissue. In contrast, the axial noncontrast single-energy CT image (*B*) obtained in a patient with long-standing Hashimoto disease demonstrates an iodine-deficient thyroid gland (*asterisks*, *B*), appearing nearly isodense to muscle, which renders differentiation of parathyroid lesions from exophytic thyroid tissue more difficult.

virtual monoenergetic imaging is an application of dual-energy CT that can be used to accentuate the conspicuity of enhancing masses on neck CT[10] as well as to increase arterial attenuation and the contrast-to-noise ratio (CNR) on CT angiography of the head and neck.[11] These applications of low-kiloelectron volt virtual monochromatic images (VMI) related to iodinated contrast media are possible because the CT attenuation of an element is maximal at or slightly above the K-edge of the element, and the K-edge of iodine is 33.2 keV.[9,12] It would, therefore, be expected that low-kiloelectron volt VMI could also be used to accentuate the attenuation of native thyroid iodine on noncontrast images (Fig 2), though formal investigation is warranted.

We hypothesized that 40-keV VMI will increase the conspicuity of thyroid tissue relative to nonthyroid tissue (eg, parathyroid lesions, muscle) on the noncontrast phase of a DECT parathyroid 4D-CT protocol, thereby facilitating discrimination of parathyroid lesions from exophytic thyroid tissue. The purpose of this study was to test our hypothesis through the quantitative assessment of Hounsfield unit attenuation and CNR on standard (70-keV) noncontrast VMI and 40-keV noncontrast VMI.

MATERIALS AND METHODS

Subjects

For this retrospective, Health Insurance Portability and Accountability Act–compliant, institutional review board–approved study, all parathyroid 4D-CT examinations performed at our institution between March 2020 and November 2020 were retrospectively reviewed ($n = 35$). Inclusion criteria were the following: 1) DECT acquisition used, 2) parathyroidectomy performed, 3) largest pathologically-proved parathyroid lesion measured at least 1 cm in the long axis, and 4) no prior thyroidectomy. Examinations not meeting all inclusion criteria were excluded.

Medical Record Review

The following data were obtained from the electronic medical record for the study cohort: age, sex, medical history of hypothyroidism, parathyroid surgery operative notes, and pathology reports for parathyroid surgical specimens.

Image Acquisition

All parathyroid 4D-CT examinations were performed on a Revolution Apex CT system (GE Healthcare) using a dual-energy acquisition. The CT acquisition parameters were as follows: 80-/140-kV(peak) simultaneous acquisition, 250–445 mA, 0.516:1 pitch, 0.5-second rotation time, 40-mm detector coverage, 2.5-mm helical section thickness, and 2.5-mm interval for each of 3 CT phases (noncontrast, 30-second postcontrast, and 60-second postcontrast). Multiplanar reconstructions of each CT phase were generated, including 0.625-mm axial 70-keV VMI and 0.625-mm axial 40-keV VMI of the noncontrast phase (reconstruction method: adaptive statistical iterative reconstruction V, 20%; convolution kernel: standard; display FOV: 22 cm for 70- and 40- keV image sets). The volume CT dose index for each CT phase ranged between 14 and 24 mGy (32-cm phantom). For comparison, a recently reported single-energy protocol performed at 140 kV(p) resulted in a volume CT dose index range of 19 to 24 mGy (32-cm phantom).[1]

Image Analysis

2D circular ROIs were drawn by a neuroradiology fellow on the 0.625-mm axial 70- and 40-keV images using our institution's PACS. An attending neuroradiologist with 4 years' experience interpreting parathyroid 4D-CT reviewed and verified all ROIs placed by the neuroradiology fellow, optimizing ROI size and position if needed. The image sets were linked so that identical ROIs could be drawn in the same location on both the 70- and 40-keV image sets. In each patient, ROIs were placed in the right and left lobes of the thyroid gland, within the right and left sternocleidomastoid muscles, within the subcutaneous fat of the midline posterior neck, and within the largest pathologically-proved parathyroid lesion (adenoma or hyperplasia). Care was taken with the placement of all ROIs to avoid confounding structures, such as thyroid nodules and blood vessels. The ROI size for the thyroid lobes and sternocleidomastoid muscles was 0.5 cm^2. ROI size for subcutaneous fat was 2.0 cm^2 in most ($n = 18$) patients, though by necessity, it was 1.0 cm^2 in 2 very thin patients. The ROI size for parathyroid lesions ranged between 0.1 and 0.83 cm^2 (median, 0.20 cm^2). The mean Hounsfield unit attenuation (SD) was recorded for each ROI.

Absolute differences in Hounsfield unit attenuation and percentage change were calculated for thyroid gland, parathyroid lesions, and sternocleidomastoid muscles at 40 keV compared with 70 keV.

The CNR of the thyroid gland relative to pathologically-proved parathyroid lesions ($CNR_{thy/par}$) of at least 1 cm was calculated using the following formula: $(ROI_{thy} - ROI_{par})/SD$, where ROI_{thy} is the mean Hounsfield unit attenuation of the thyroid lobes, ROI_{par} is the mean Hounsfield unit attenuation of the parathyroid lesion, and SD is the Hounsfield unit attenuation SD of subcutaneous fat.

The CNR of the thyroid gland relative to the sternocleidomastoid muscles ($CNR_{thy/scm}$) was calculated for each patient using the

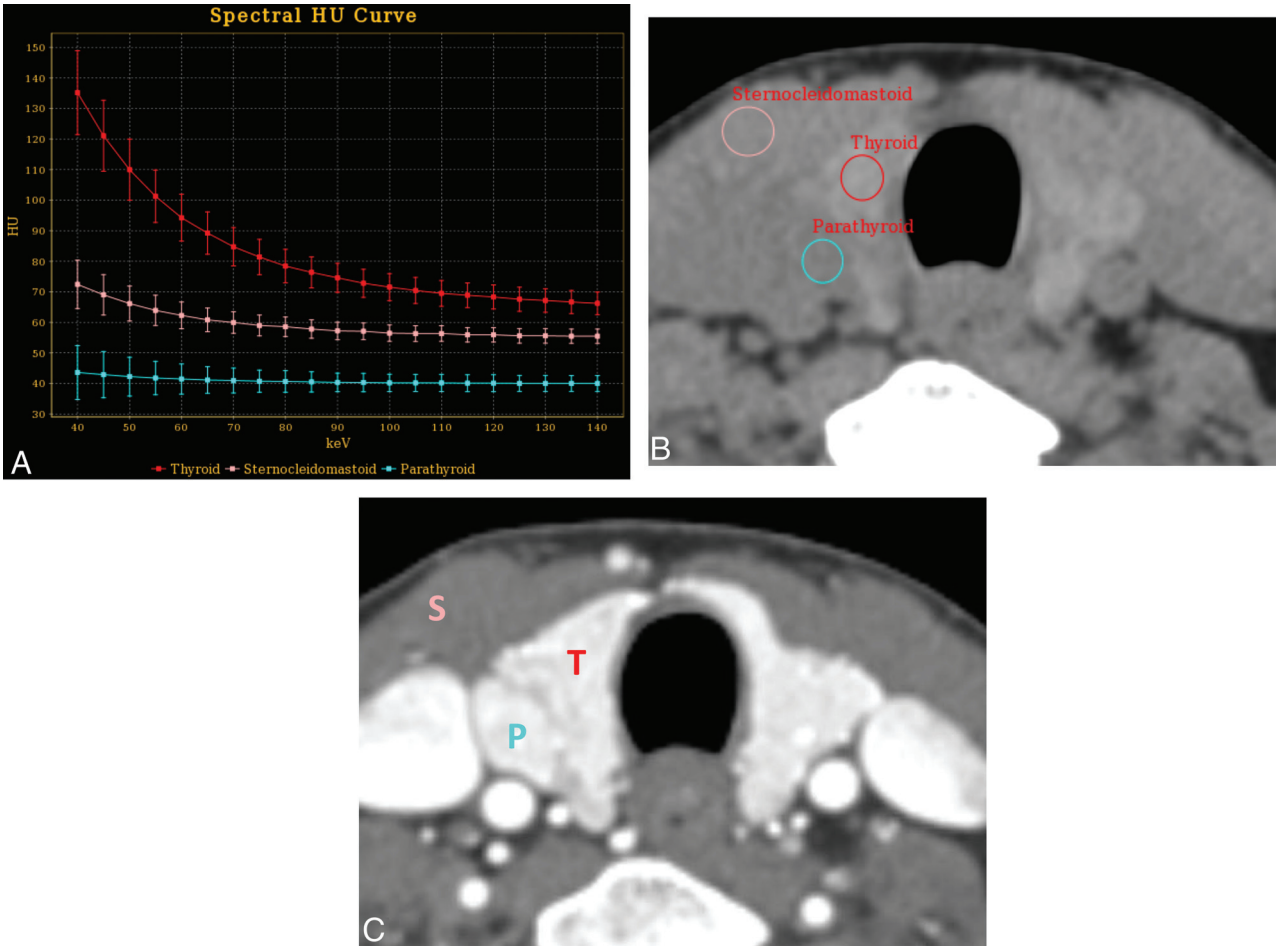

FIG 2. Virtual monoenergetic spectral curves (*A*) demonstrate noncontrast Hounsfield unit attenuation as a function of kiloelectron volts for the thyroid gland (red), sternocleidomastoid muscle (pink), and pathologically-proved parathyroid adenoma (blue) generated from ROIs placed on an axial noncontrast 70-keV virtual monoenergetic image (*B*) in a 56-year-old woman with primary hyperparathyroidism. The noncontrast Hounsfield unit attenuation difference between thyroid and the other tissues of interest is maximal at 40 keV. Corresponding axial arterial phase CT image (*C*) is also provided for comparison. T indicates thyroid; S, sternocleidomastoid; P, parathyroid.

Table 1: Characteristics of the study group

Characteristics	
Age (median) (range) (yr)	63 (33–81)
Sex	
Male	9
Female	11
Operative findings	
Single-gland disease	16
Multigland disease	4
Concurrent hypothyroidism	
Yes	3
No	17

following formula: $(ROI_{thy} - ROI_{scm})/SD$, where ROI_{scm} is the mean Hounsfield unit attenuation of the sternocleidomastoid muscles.

Statistical Analysis

Descriptive analyses were performed using absolute and relative frequencies for categoric variables and median and interquartile range (IQR) for continuous variables, respectively. The Wilcoxon signed rank test was used to compare differences in Hounsfield unit attenuation, CNR, and image noise between the 70- and 40-keV images. All analyses were performed with Excel 2016 (Microsoft) and Matlab (MathWorks). A P value $< .05$ indicated a statistically significant difference.

RESULTS

Subjects

Of the 35 parathyroid 4D-CT examinations reviewed, 3 examinations were excluded because a DECT acquisition was not used, 8 were excluded because the patient had not yet undergone parathyroidectomy, 2 were excluded because the largest pathologically-proved parathyroid lesion did not meet the 1-cm minimum size threshold of this study, and 2 were excluded due to prior thyroidectomy. This process yielded 20 parathyroid 4D-CT examinations in the study cohort. Characteristics of the study group are summarized in Table 1.

Histopathologic analysis of the surgical specimens from these 20 patients revealed a total of 28 pathologically-proved parathyroid lesions, 26 (93%) of which were identified and described on preoperative CT. The 2 parathyroid lesions not identified on preoperative CT both measured <1 cm in maximum dimension and occurred in 2 different patients with multiglandular disease. In

Table 2: Summary of differences in Hounsfield unit attenuation, contrast-to-noise, and image noise at 70 and 40 keV

	40 keV (Median) (IQR)	70 keV (Median) (IQR)	Difference (40-70 keV) (Median) (IQR)	*P*	Comparison (*P*)
Hounsfield unit attenuation					
Thyroid					
Absolute (HU)	158 (133–264)	84 (74–113)	+67 (55–142)	<.001	Par
				<.001	SCM
% Change			+89% (66–123)	<.001	Par
				<.001	SCM
Parathyroid					
Absolute (HU)	42 (29–59)	32 (22–41)	+9 (4–17)	<.001	Thy
				.22	SCM
% Change			+29% (13–58)	<.001	Thy
				.09	SCM
Sternocleidomastoid					
Absolute (HU)	67 (63–75)	57 (54–59)	+11 (10–16)	<.001	Thy
				.22	Par
% Change			+22% (17–28)	<.001	Thy
				.09	Par
Contrast-to-noise					
Thy/Par	4.7 (3.3–6.0)	3.8 (2.4–4.8)	+0.8 (0.2–1.2)	<.001	
Thy/SCM	3.6 (1.7–5.0)	2.3 (0.9–3.1)	+1.3 (0.7–1.9)	<.001	
Image noise (HU)	32 (23–37)	16 (12–19)	+14 (11–20)	<.001	

Note:—Thy indicates thyroid; Par, parathyroid; SCM, sternocleidomastoid.

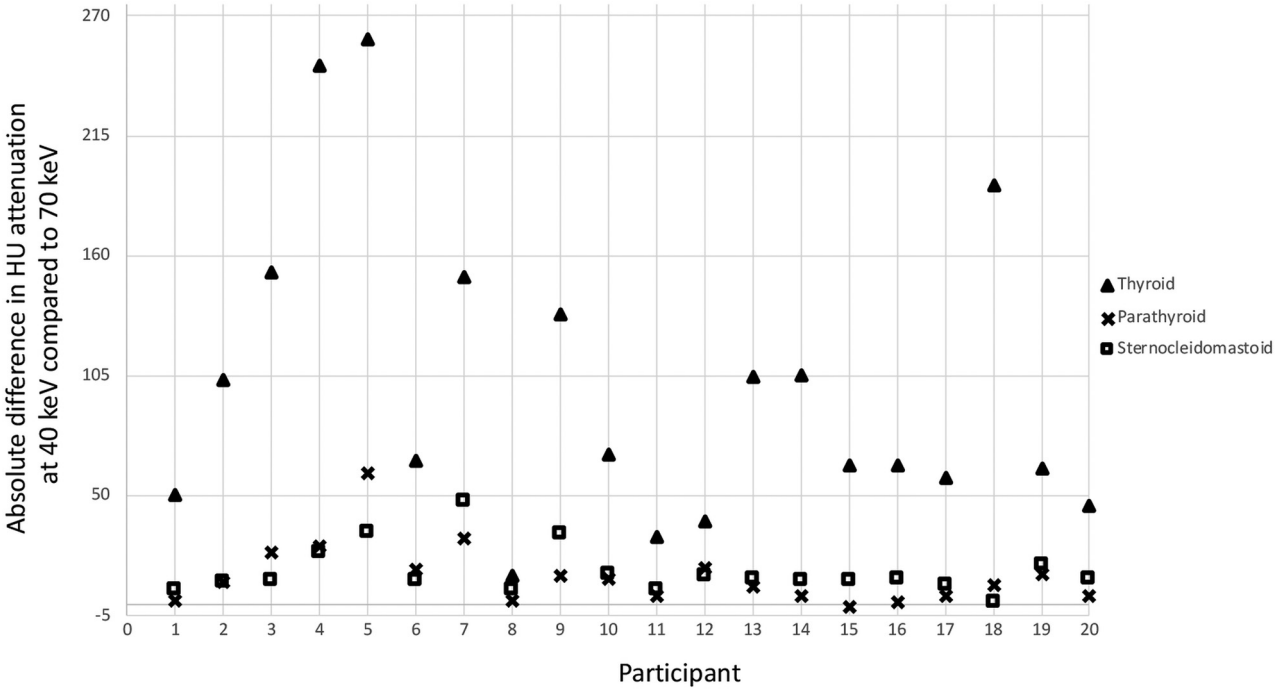

FIG 3. Dot plot demonstrates the absolute difference in Hounsfield unit attenuation between 40 keV and 70 keV for thyroid gland (*triangle*), parathyroid lesions (*X*), and sternocleidomastoid muscles (*square*) in each of the 20 study participants.

one of these patients, 2 of 3 proved parathyroid lesions were described on preoperative CT, and 3 of 4 proved parathyroid lesions were described on preoperative CT in the other.

Image Analysis

Quantitative data related to Hounsfield unit attenuation and percentage change, CNR, and image noise are summarized in Table 2.

Attenuation and Percentage Change. Thyroid gland, parathyroid lesion, and sternocleidomastoid muscle Hounsfield unit attenuation increased at 40 keV compared with 70 keV in 20/20 (100%) patients, 19/20 (95%) patients, and 20/20 (100%) patients, respectively. For all 20 patients, the absolute Hounsfield unit increase (Fig 3) and percentage Hounsfield unit increase at 40 keV relative to 70 keV was greater for thyroid than for parathyroid lesions and for the sternocleidomastoid muscles. One parathyroid lesion

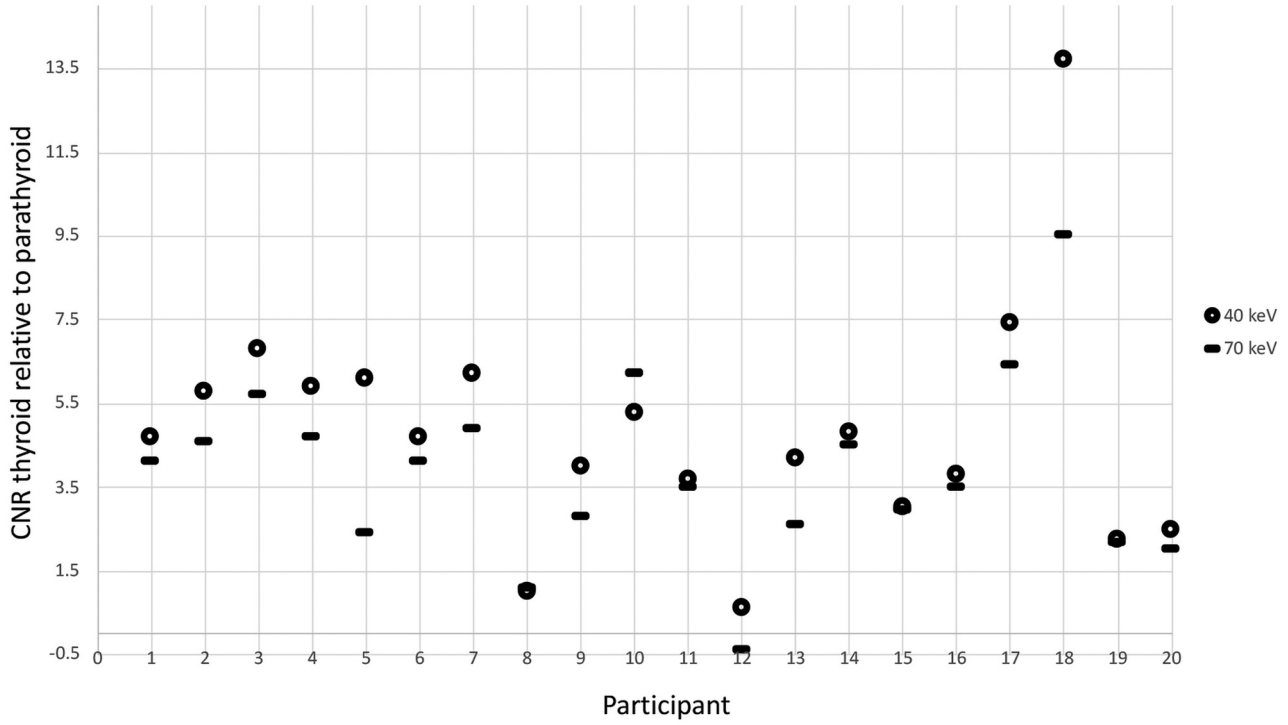

FIG 4. Dot plot demonstrates contrast-to-noise ratios between the thyroid gland and pathologically-proved parathyroid lesions at 40 keV (*circle*) and 70 keV (*line*) for each of the 20 study participants.

(participant No. 15, Fig 3) demonstrated a 5% decrease in Hounsfield unit attenuation at 40 keV compared with 70 keV.

The median absolute difference in Hounsfield unit attenuation at 40 keV compared with 70 keV was +67 HU (IQR, 55–142 HU) for the thyroid gland, +9 HU (IQR, 4–17 HU) for parathyroid lesions, and +11 HU (IQR, 10–16 HU) for the sternocleidomastoid muscles. The observed differences in absolute Hounsfield unit attenuation increase for thyroid compared with parathyroid lesions ($P < .001$) and sternocleidomastoid muscles ($P < .001$) were statistically significant. There was no significant difference in the absolute Hounsfield unit increase between parathyroid lesions and sternocleidomastoid muscles ($P = .22$).

The median percentage difference in Hounsfield unit attenuation at 40 keV compared with 70 keV was +89% (IQR, +66% to +123%) for the thyroid gland, +29% (IQR, +13% to +58%) for parathyroid lesions, and +22% (IQR, +17% to +28%) for the sternocleidomastoid muscles. The observed differences in the percentage increase in Hounsfield unit attenuation for thyroid compared with parathyroid lesions ($P < .001$) and sternocleidomastoid muscles ($P < .001$) were statistically significant. There was no significant difference in the percentage increase in Hounsfield unit attenuation between parathyroid lesions and sternocleidomastoid muscles ($P = .09$).

Contrast-to-Noise. The CNR of the thyroid gland relative to parathyroid lesions ($CNR_{thy/par}$) increased on 40-keV VMI compared with standard 70-keV VMI in 18/20 (90%) patients (Fig 4). The median $CNR_{thy/par}$ at 40 keV was 4.7 (IQR, 3.3–6.0) compared with 3.8 (IQR, 2.4–4.8) at 70 keV, and the median increase in $CNR_{thy/par}$ at 40 keV compared with 70 keV was 0.8 (IQR, 0.2–1.2; $P < .001$). $CNR_{thy/par}$ decreased at 40 keV relative to 70 keV in participants Nos. 8 and 10 (Fig 4), one of whom (participant No. 8) had a minimal increase in thyroid attenuation at 40 keV and known hypothyroidism. In the other (participant No. 10), the observed percentage increase in thyroid attenuation at 40 keV relative to 70 keV was similar (rather than disproportionate) to the percentage increase in parathyroid lesion attenuation.

The CNR of the thyroid gland relative to the sternocleidomastoid muscles ($CNR_{thy/scm}$) increased on 40-keV VMI compared with standard 70-keV VMI in 20/20 (100%) patients. The median $CNR_{thy/scm}$ at 40 keV was 3.6 (IQR, 1.7–5.0) compared with 2.3 (IQR, 0.9–3.1) at 70 keV, and the median increase in $CNR_{thy/scm}$ at 40 keV compared with 70 keV was 1.3 (IQR, 0.7–1.9; $P < .001$).

Image Noise. Image noise, defined as the Hounsfield unit attenuation SD of subcutaneous fat for the purposes of this study, increased at 40 keV compared with 70 keV in 20/20 (100%) patients. The median image noise at 40 keV was 32 HU (IQR, 23–37 HU) compared with 16 HU (IQR, 12–19 HU) at 70 keV, and the median noise increase at 40 keV compared with 70 keV was 14 HU (IQR, 11–20 HU; $P < .001$).

DISCUSSION

Numerous applications of DECT have been described in head and neck imaging.[10,13-21] Previously published studies of dual-energy parathyroid CT have primarily focused on the potential for radiation dose reduction using virtual noncontrast images to eliminate the standard noncontrast phase[22,23] and on describing quantitative dual-energy characteristics of parathyroid adenomas, thyroid parenchyma, and lymph nodes on postcontrast phases.[24,25] The authors are aware of 1 previous study that evaluated dual-energy

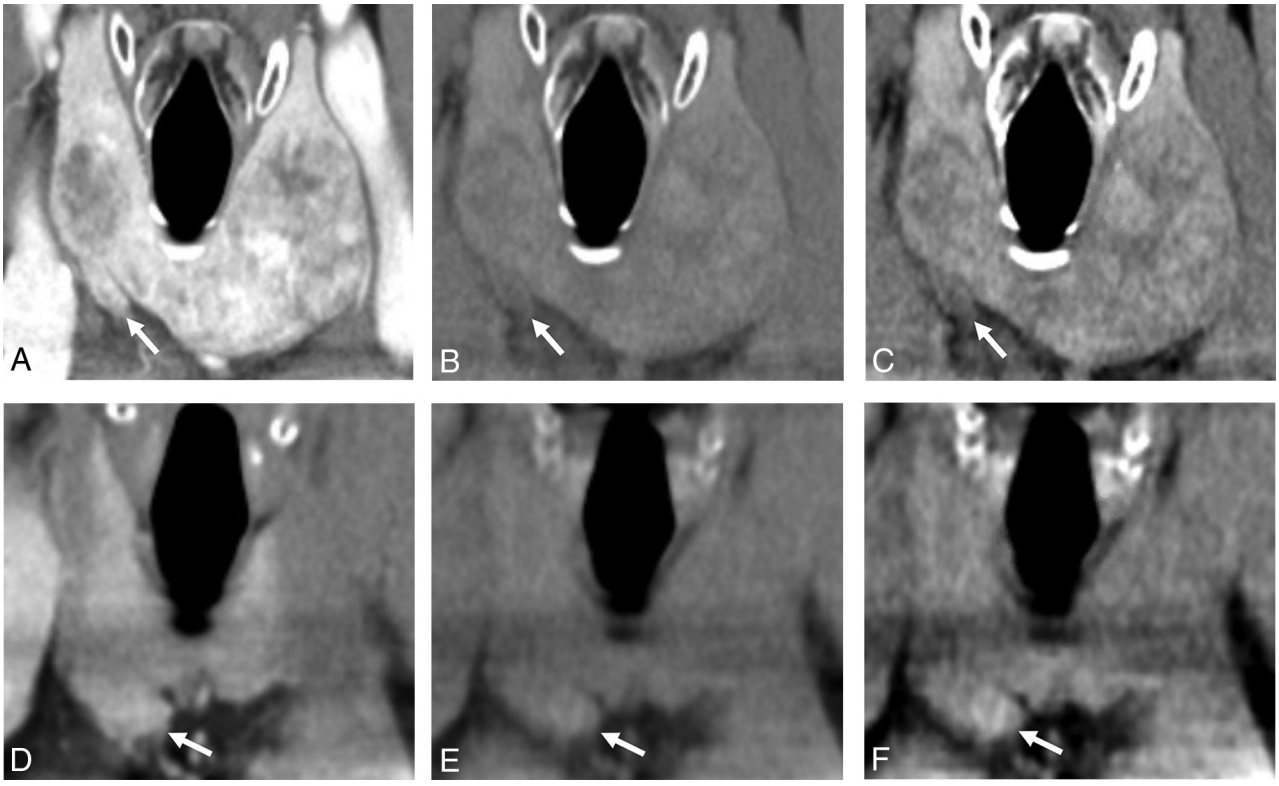

FIG 5. Coronal arterial phase (*A*), noncontrast 70-keV (*B*), and noncontrast 40-keV (*C*) images demonstrate a pathologically-proved right inferior parathyroid adenoma (*arrows*). Because the parathyroid adenoma appears isodense to the adjacent thyroid gland on the arterial phase image, it is uncertain whether the finding represents a parathyroid lesion or exophytic thyroid tissue. The parathyroid adenoma appears slightly hypoattenuating to the thyroid parenchyma on the standard (70-keV) noncontrast image; however, this attenuation difference is accentuated on the 40-keV image, indicating that the finding represents a parathyroid lesion rather than exophytic thyroid tissue. In contrast, coronal arterial phase (*D*), noncontrast 70-keV (*E*), and noncontrast 40-keV (*F*) images from a different patient demonstrate exophytic thyroid tissue (*arrows*) arising from the lower pole of the right thyroid lobe. On the arterial phase image alone, it is uncertain whether the finding represents exophytic thyroid tissue or a right inferior parathyroid lesion. Although the finding is isodense relative to the thyroid gland on the 70-keV noncontrast image, some uncertainty persists because of the nearly isoattenuating appearance of the thyroid gland relative to adjacent muscle, suggesting decreased iodine content from chronic thyroid disease. The 40-keV noncontrast image demonstrates substantially increased attenuation of the finding comparable with the increased attenuation of the remainder of the thyroid gland, indicating that the finding of interest represents exophytic thyroid tissue rather than a parathyroid lesion. In this patient, a biochemical cure was achieved with removal of a pathologically-proved parathyroid adenoma identified elsewhere in the neck (not shown), confirming that the finding depicted in images *D*, *E*, and *F* is indeed not a parathyroid lesion. Section thickness (2 mm), window level (40 HU), and window width (400 HU) are identical for all 6 images.

noncontrast parathyroid CT images obtained on a dual-source system using 90-keV, 150-keV, and mixed images (dual-energy composition factor, 0.8), but 40-keV VMI were not specifically evaluated in this previous investigation.[25]

Our study compared the conspicuity of thyroid tissue relative to pathologically-proved parathyroid lesions and muscle on 40-keV noncontrast VMI and standard 70-keV noncontrast VMI obtained on a fast-kiloelectron volt switching system and found statistically significant increase in CNR at 40 keV compared with the 70 keV standard. These findings support our hypothesis that noncontrast 40-keV VMI facilitate the differentiation of parathyroid lesions from exophytic thyroid tissue by accentuating the attenuation of iodine within thyroid tissue that is absent from parathyroid tissue (Fig 5). Although the attenuation of thyroid, parathyroid, and muscle generally increased at 40 keV relative to 70 keV, the increase in attenuation of the thyroid gland was disproportionately greater in most subjects because of the proximity to the K-edge (33.2 keV) of iodine. Although the cause of the observed 5% decrease in Hounsfield unit attenuation of 1 parathyroid adenoma at 40 keV compared with 70 keV is uncertain, this finding may relate to intralesional fat deposition,[1] given that the attenuation of fat is known to decrease at low kiloelectron volts.[12]

Localization confidence is highly desirable in parathyroid imaging. Not uncommonly, multiple parathyroid imaging studies are requested in an attempt to maximize the surgeon's confidence in localization through concordant imaging results. The degree of diagnostic confidence or lack thereof carries implications for the operative plan, and in certain high-risk scenarios (eg, the reoperative neck), it may determine whether an operation is offered at all.[1] Although radiologists' confidence was not directly tested in this study, it has been our clinical experience in interpreting dual-energy parathyroid CT that noncontrast 40-keV VMI facilitate more confident differentiation of parathyroid lesions from exophytic thyroid tissue. Some authors have advocated for omitting the true noncontrast phase as nonessential.[23,26,27] However, in our experience, the true noncontrast phase is indispensable because it improves sensitivity by enabling detection of parathyroid lesions

that would be otherwise overlooked (eg, abutting and isoattenuating to thyroid on contrast-enhanced phases), and it decreases false-positive candidate lesions by facilitating accurate characterization of exophytic thyroid tissue on the basis of intrinsic iodine content. To minimize adverse effects of the additional 40-keV VMI series on workflow, the 40-keV VMI are automatically generated and sent to the PACS at our institution, thus requiring no manual processing by the radiologist.

There are limitations to this study. First, a small number of patients were included in the cohort, which relates to our recent implementation of dual-energy parathyroid 4D-CT and our requirement that only data from pathologically-proved parathyroid lesions be used. Second, all parathyroid 4D-CTs were acquired with a single vendor's DECT system so that our findings are not necessarily generalizable to other vendors' DECT systems, though the underlying physical principles should be the same. This study investigated the potential value of noncontrast 40-keV VMI for the focused task of determining whether a tissue of interest is likely to be thyroid, and it was not intended to be a comprehensive assessment of image quality.

Note that image noise, as estimated by the Hounsfield unit attenuation SD of subcutaneous fat, was significantly higher at 40 keV. This phenomenon of increased noise on 40-keV VMI has also been observed in a DECT phantom study[28] and is in keeping with the progressive increase in image noise observed on low-kiloelectron volt VMI described in a previous study of neck DECT examinations also performed using a fast-kiloelectron volt switching system.[29] In the future, image noise in 40- keV VMI could likely be decreased with the addition of noise-reducing reconstruction algorithms;[30] however, such algorithms were not a part of the current study. Furthermore, it is possible that additional gains in CNR could be achieved at a kiloelectron volt intermediate between 40 and 70 keV by balancing the benefit of the disproportionate increase in thyroid iodine attenuation at a low kiloelectron volt against the cost of increased noise. Although in our clinical experience the noncontrast 40-keV VMI increased the radiologist's interpretation confidence, the overall assessment should continue to incorporate other candidate parathyroid lesion features (eg, morphology, enhancement characteristics, polar vessel sign). Finally, whether there is a positive impact of 40-keV VMI on interpretation accuracy remains undetermined.

CONCLUSIONS

Compared with standard (70-keV VMI) noncontrast images, 40-keV VMI significantly increase Hounsfield unit attenuation and CNR of thyroid tissue relative to parathyroid lesions and sternocleidomastoid muscle. Therefore, 40-keV VMI facilitate differentiation of parathyroid lesions from exophytic thyroid tissue on noncontrast images, which is particularly useful for the subset of parathyroid lesions that exhibit isoattenuation to thyroid parenchyma on the arterial and venous phases of a parathyroid 4D-CT protocol and could be missed without the noncontrast CT phase.

REFERENCES

1. Bunch PM, Randolph GW, Brooks JA, et al. **Parathyroid 4D CT: what the surgeon wants to know.** *Radiographics* 2020;40:1383–94 CrossRef Medline
2. Perrier N, Parangi S. **Minimally invasive single gland parathyroid exploration.** In: Randolph G, ed. *Surgery of the Thyroid and Parathyroid Glands*. 2nd ed. Elsevier 2012; 580–89
3. Minisola S, Cipriani C, Diacinti D, et al. **Imaging of the parathyroid glands in primary hyperparathyroidism.** *Eur J Endocrinol* 2016;174: D1–8 CrossRef Medline
4. Hoang JK, Williams K, Gaillard F, et al. **Parathyroid 4D-CT: multi-institutional international survey of use and trends.** *Otolaryngol Head Neck Surg* 2016;155:956–60 CrossRef Medline
5. Bunch PM, Kelly HR. **Preoperative imaging techniques in primary hyperparathyroidism: a review.** *JAMA Otolaryngol Head Neck Surg* 2018;144:929–37 CrossRef Medline
6. Bahl M, Sepahdari AR, Sosa JA, et al. **Parathyroid adenomas and hyperplasia on four-dimensional CT scans: three patterns of enhancement relative to the thyroid gland justify a three-phase protocol.** *Radiology* 2015;277:454–62 CrossRef Medline
7. Bentrem DJ, Angelos P, Talamonti MS, et al. **Is preoperative investigation of the thyroid justified in patients undergoing parathyroidectomy for hyperparathyroidism?** *Thyroid* 2002;12:1109–12 CrossRef Medline
8. Jovanovic MD, Zivaljevic VR, Diklic AD, et al. **Surgical treatment of concomitant thyroid and parathyroid disorders: analysis of 4882 cases.** *Eur Arch Otorhinolaryngol* 2017;274:997–1004 CrossRef Medline
9. Sachs JR, West TG, Lack CM, et al. **How to incorporate dual-energy computed tomography into your neuroradiology practice: questions and answers.** *J Comput Assist Tomogr* 2018;42:824–30 CrossRef Medline
10. Forghani R, Kelly HR, Curtin HD. **Applications of dual-energy computed tomography for the evaluation of head and neck squamous cell carcinoma.** *Neuroimaging Clin N Am* 2017;27:445–59 CrossRef Medline
11. Neuhaus V, Große Hokamp N, Abdullayev N, et al. **Comparison of virtual monoenergetic and polyenergetic images reconstructed from dual-layer detector CT angiography of the head and neck.** *Eur Radiol* 2018;28:1102–10 CrossRef Medline
12. Potter CA, Sodickson AD. **Dual-energy CT in emergency neuroimaging: added value and novel applications.** *Radiographics* 2016;36:2186–98 CrossRef Medline
13. Vogl TJ, Schulz B, Bauer RW, et al. **Dual-energy CT applications in head and neck imaging.** *AJR Am J Roentgenol* 2012;199:S34–39 CrossRef Medline
14. Tawfik AM, Razek AA, Kerl JM, et al. **Comparison of dual-energy CT-derived iodine content and iodine overlay of normal, inflammatory and metastatic squamous cell carcinoma cervical lymph nodes.** *Eur Radiol* 2014;24:574–80 CrossRef Medline
15. Liu X, Ouyang D, Li H, et al. **Papillary thyroid cancer: dual-energy spectral CT quantitative parameters for preoperative diagnosis of metastasis to the cervical lymph nodes.** *Radiology* 2015;275:167–76 CrossRef Medline
16. Yamauchi H, Buehler M, Goodsitt MM, et al. **Dual-energy CT-based differentiation of benign posttreatment changes from primary or recurrent malignancy of the head and neck: comparison of spectral Hounsfield units at 40 and 70 keV and iodine concentration.** *AJR Am J Roentgenol* 2016;206:580–87 CrossRef
17. Kuno H, Sakamaki K, Fujii S, et al. **Comparison of MR imaging and dual-energy CT for the evaluation of cartilage invasion by laryngeal and hypopharyngeal squamous cell carcinoma.** *AJNR Am J Neuroradiol* 2018;39:524–31 CrossRef Medline
18. Forghani R, Chatterjee A, Reinhold C, et al. **Head and neck squamous cell carcinoma: prediction of cervical lymph node metastasis by dual-energy CT texture analysis with machine learning.** *Eur Radiol* 2019;29:6172–81 CrossRef Medline

19. Lee DH, Lee YH, Seo HS, et al. **Dual-energy CT iodine quantification for characterizing focal thyroid lesions.** *Head Neck* 2019;41:1024–31 CrossRef Medline
20. Timmer VCML, Kroonenburgh AMJLV, Henneman WJP, et al. **Detection of bone marrow edema in the head and neck with dual-energy CT: ready for clinical use?** *AJR Am J Roentgenol* 2020;214:893–99 CrossRef Medline
21. Sachs JR, Lack CM, West TG, et al. **Unique characteristics of intravitreal silicone oil on dual-energy computed tomography.** *J Comput Assist Tomogr* 2020;44:370–73 CrossRef Medline
22. Roskies M, Liu X, Hier MP, et al. **3-phase dual-energy CT scan as a feasible salvage imaging modality for the identification of non-localizing parathyroid adenomas: a prospective study.** *J Otolaryngol Head Neck Surg* 2015;44:44 CrossRef Medline
23. Leiva-Salinas C, Flors L, Durst CR, et al. **Detection of parathyroid adenomas using a monophasic dual-energy computed tomography acquisition: diagnostic performance and potential radiation dose reduction.** *Neuroradiology* 2016;58:1135–41 CrossRef Medline
24. Forghani R, Roskies M, Liu X, et al. **Dual-energy CT characteristics of parathyroid adenomas on 25-and 55-second 4D-CT acquisitions: preliminary experience.** *J Comput Assist Tomogr* 2016;40:806–14 CrossRef Medline
25. Woisetschläger M, Gimm O, Johansson K, et al. **Dual energy 4D-CT of parathyroid adenomas not clearly localized by sestamibi scintigraphy and ultrasonography: a retrospective study.** *Eur J Radiol* 2020;124:108821 CrossRef Medline
26. Raghavan P, Durst CR, Ornan DA, et al. **Dynamic CT for parathyroid disease: are multiple phases necessary?** *AJNR Am J Neuroradiol* 2014;35:1959–64 CrossRef Medline
27. Morón F, Delumpa A, Chetta J, et al. **Single phase computed tomography is equivalent to dual phase method for localizing hyperfunctioning parathyroid glands in patients with primary hyperparathyroidism: a retrospective review.** *PeerJ* 2017;5:e3586 CrossRef Medline
28. Matsumoto K, Jinzaki M, Tanami Y, et al. **Virtual monochromatic spectral imaging with fast kilovoltage switching: improved image quality as compared with that obtained with conventional 120-kVp CT.** *Radiology* 2011;259:257–62 CrossRef Medline
29. Lam S, Gupta R, Levental M, et al. **Optimal virtual monochromatic images for evaluation of normal tissues and head and neck cancer using dual-energy CT.** *AJNR Am J Neuroradiol* 2015;36:1518–24 CrossRef Medline
30. Jensen CT, Liu X, Tamm EP, et al. **Image quality assessment of abdominal CT by use of new deep learning image reconstruction: initial experience.** *AJR Am J Roentgenol* 2020;215:50–57 CrossRef Medline